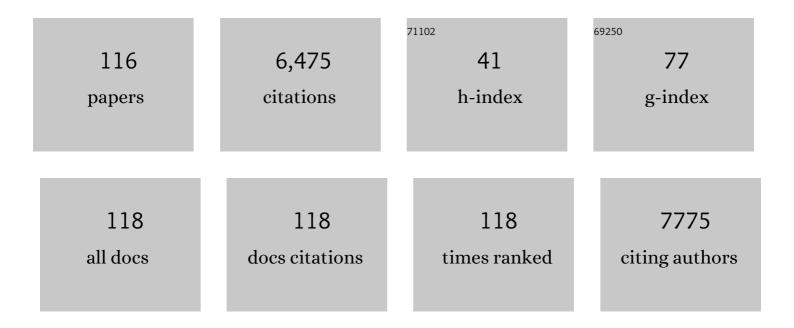
## Jin-Hong Park

List of Publications by Year in descending order

Source: https://exaly.com/author-pdf/1629719/publications.pdf Version: 2024-02-01



#	Article	IF	CITATIONS
1	Artificial optic-neural synapse for colored and color-mixed pattern recognition. Nature Communications, 2018, 9, 5106.	12.8	462
2	Layer-controlled CVD growth of large-area two-dimensional MoS <sub>2</sub> films. Nanoscale, 2015, 7, 1688-1695.	5.6	387
3	Phosphorene/rhenium disulfide heterojunction-based negative differential resistance device for multi-valued logic. Nature Communications, 2016, 7, 13413.	12.8	332
4	Surface group modification and carrier transport properties of layered transition metal carbides (Ti <sub>2</sub> CT <sub>x</sub> , T: –OH, –F and –O). Nanoscale, 2015, 7, 19390-19396.	5.6	285
5	Optoelectronic Synapse Based on IGZOâ€Alkylated Graphene Oxide Hybrid Structure. Advanced Functional Materials, 2018, 28, 1804397.	14.9	280
6	Highâ€Performance Transition Metal Dichalcogenide Photodetectors Enhanced by Selfâ€Assembled Monolayer Doping. Advanced Functional Materials, 2015, 25, 4219-4227.	14.9	247
7	<b>An Ultrahighâ€Performance Photodetector based on a Perovskite–Transitionâ€Metalâ€Dichalcogenide Hybrid Structure</b> . Advanced Materials, 2016, 28, 7799-7806.	21.0	242
8	Highâ€Performance 2D Rhenium Disulfide (ReS <sub>2</sub> ) Transistors and Photodetectors by Oxygen Plasma Treatment. Advanced Materials, 2016, 28, 6985-6992.	21.0	209
9	MXene Electrode for the Integration of WSe <sub>2</sub> and MoS <sub>2</sub> Field Effect Transistors. Advanced Functional Materials, 2016, 26, 5328-5334.	14.9	198
10	Plasma-Treated Thickness-Controlled Two-Dimensional Black Phosphorus and Its Electronic Transport Properties. ACS Nano, 2015, 9, 8729-8736.	14.6	166
11	Controllable Nondegenerate p-Type Doping of Tungsten Diselenide by Octadecyltrichlorosilane. ACS Nano, 2015, 9, 1099-1107.	14.6	139
12	A Highâ€Performance WSe <sub>2</sub> / <i>h</i> â€BN Photodetector using a Triphenylphosphine (PPh <sub>3</sub> )â€Based nâ€Đoping Technique. Advanced Materials, 2016, 28, 4824-4831.	21.0	139
13	Vertical organic synapse expandable to 3D crossbar array. Nature Communications, 2020, 11, 4595.	12.8	130
14	Artificial van der Waals hybrid synapse and its application to acoustic pattern recognition. Nature Communications, 2020, 11, 3936.	12.8	125
15	Electronic and Optoelectronic Devices based on Twoâ€Dimensional Materials: From Fabrication to Application. Advanced Electronic Materials, 2017, 3, 1600364.	5.1	123
16	Perovskite-related (CH <sub>3</sub> NH <sub>3</sub> ) <sub>3</sub> Sb <sub>2</sub> Br <sub>9</sub> for forming-free memristor and low-energy-consuming neuromorphic computing. Nanoscale, 2019, 11, 6453-6461.	5.6	121
17	Recent Progress in Artificial Synapses Based on Two-Dimensional van der Waals Materials for Brain-Inspired Computing. ACS Applied Electronic Materials, 2020, 2, 371-388.	4.3	110
18	Solar-stimulated optoelectronic synapse based on organic heterojunction with linearly potentiated synaptic weight for neuromorphic computing. Nano Energy, 2019, 66, 104095.	16.0	100

#	Article	IF	CITATIONS
19	Modulation of the Electronic Properties of MXene (Ti <sub>3</sub> C <sub>2</sub> T <sub><i>x</i></sub> ) <i>via</i> Surface-Covalent Functionalization with Diazonium. ACS Nano, 2021, 15, 1388-1396.	14.6	100
20	Extremely Large Gate Modulation in Vertical Graphene/WSe <sub>2</sub> Heterojunction Barristor Based on a Novel Transport Mechanism. Advanced Materials, 2016, 28, 5293-5299.	21.0	92
21	2D–Organic Hybrid Heterostructures for Optoelectronic Applications. Advanced Materials, 2019, 31, e1803831.	21.0	86
22	n- and p-Type Doping Phenomenon by Artificial DNA and M-DNA on Two-Dimensional Transition Metal Dichalcogenides. ACS Nano, 2014, 8, 11603-11613.	14.6	85
23	High-specific-power flexible transition metal dichalcogenide solar cells. Nature Communications, 2021, 12, 7034.	12.8	84
24	Recent progress in Van der Waals (vdW) heterojunction-based electronic and optoelectronic devices. Carbon, 2018, 133, 78-89.	10.3	83
25	Light-Triggered Ternary Device and Inverter Based on Heterojunction of van der Waals Materials. ACS Nano, 2017, 11, 6319-6327.	14.6	78
26	Broad Detection Range Rhenium Diselenide Photodetector Enhanced by (3â€Aminopropyl)Triethoxysilane and Triphenylphosphine Treatment. Advanced Materials, 2016, 28, 6711-6718.	21.0	72
27	Extremely Low Contact Resistance on Graphene through nâ€īype Doping and Edge Contact Design. Advanced Materials, 2016, 28, 864-870.	21.0	70
28	A multiple negative differential resistance heterojunction device and its circuit application to ternary static random access memory. Nanoscale Horizons, 2020, 5, 654-662.	8.0	70
29	Plasmonic Transition Metal Carbide Electrodes for High-Performance InSe Photodetectors. ACS Nano, 2019, 13, 8804-8810.	14.6	69
30	Ferroelectric polymer-based artificial synapse for neuromorphic computing. Nanoscale Horizons, 2021, 6, 139-147.	8.0	68
31	A Bioinspired Stretchable Sensoryâ€Neuromorphic System. Advanced Materials, 2021, 33, e2104690.	21.0	67
32	Highly Efficient Infrared Photodetection in a Gate ontrollable Van der Waals Heterojunction with Staggered Bandgap Alignment. Advanced Science, 2018, 5, 1700423.	11.2	66
33	Ultrasensitive MoS2 photodetector by serial nano-bridge multi-heterojunction. Nature Communications, 2019, 10, 4701.	12.8	66
34	An Optogeneticsâ€Inspired Flexible van der Waals Optoelectronic Synapse and its Application to a Convolutional Neural Network. Advanced Materials, 2021, 33, e2102980.	21.0	65
35	Wide-Range Controllable n-Doping of Molybdenum Disulfide (MoS <sub>2</sub> ) through Thermal and Optical Activation. ACS Nano, 2015, 9, 2368-2376.	14.6	60
36	Transitionâ€Metalâ€Carbide (Mo <sub>2</sub> C) Multiperiod Gratings for Realization of Highâ€Sensitivity and Broadâ€Spectrum Photodetection. Advanced Functional Materials, 2019, 29, 1905384.	14.9	57

#	Article	IF	CITATIONS
37	Trap-induced photoresponse of solution-synthesized MoS <sub>2</sub> . Nanoscale, 2016, 8, 9193-9200.	5.6	52
38	Gate-Tunable Synaptic Dynamics of Ferroelectric-Coupled Carbon-Nanotube Transistors. ACS Applied Materials & Interfaces, 2020, 12, 4707-4714.	8.0	51
39	Two-Dimensional CIPS-InSe van der Waal Heterostructure Ferroelectric Field Effect Transistor for Nonvolatile Memory Applications. ACS Nano, 2022, 16, 5418-5426.	14.6	48
40	Highly Sensitive and Reusable Membraneless Field-Effect Transistor (FET)-Type Tungsten Diselenide (WSe <sub>2</sub> ) Biosensors. ACS Applied Materials & Interfaces, 2018, 10, 17639-17645.	8.0	44
41	Nanostructured encapsulation coverglasses with wide-angle broadband antireflection and self-cleaning properties for Ill–V multi-junction solar cell applications. Solar Energy Materials and Solar Cells, 2014, 120, 555-560.	6.2	42
42	Ferroelectric Fieldâ€Effectâ€Transistor Integrated with Ferroelectrics Heterostructure. Advanced Science, 2022, 9, e2200566.	11.2	42
43	Fluorine passivation of vacancy defects in bulk germanium for Ge metal-oxide-semiconductor field-effect transistor application. Applied Physics Letters, 2012, 101, 072104.	3.3	41
44	Flexible artificial Si-In-Zn-O/ion gel synapse and its application to sensory-neuromorphic system for sign language translation. Science Advances, 2021, 7, eabg9450.	10.3	41
45	Self-Assembled Layer (SAL)-Based Doping on Black Phosphorus (BP) Transistor and Photodetector. ACS Photonics, 2017, 4, 1822-1830.	6.6	39
46	Double Negative Differential Transconductance Characteristic: From Device to Circuit Application toward Quaternary Inverter. Advanced Functional Materials, 2019, 29, 1905540.	14.9	39
47	A Neuromorphic Device Implemented on a Salmonâ€DNA Electrolyte and its Application to Artificial Neural Networks. Advanced Science, 2019, 6, 1901265.	11.2	38
48	Specific Contact Resistivity Reduction Through Ar Plasma-Treated TiO <sub>2â^'x</sub> Interfacial Layer to Metal/Ge Contact. IEEE Electron Device Letters, 2014, 35, 1076-1078.	3.9	34
49	MXenes for future nanophotonic device applications. Nanophotonics, 2020, 9, 1831-1853.	6.0	31
50	Ultra-low Doping on Two-Dimensional Transition Metal Dichalcogenides using DNA Nanostructure Doped by a Combination of Lanthanide and Metal Ions. Scientific Reports, 2016, 6, 20333.	3.3	30
51	Stable and Reversible Triphenylphosphine-Based n-Type Doping Technique for Molybdenum Disulfide (MoS <sub>2</sub> ). ACS Applied Materials & Interfaces, 2018, 10, 32765-32772.	8.0	28
52	Rhenium Diselenide (ReSe <sub>2</sub> ) Nearâ€Infrared Photodetector: Performance Enhancement by Selective pâ€Doping Technique. Advanced Science, 2019, 6, 1901255.	11.2	28
53	Negative differential transconductance device with a stepped gate dielectric for multi-valued logic circuits. Nanoscale Horizons, 2020, 5, 1378-1385.	8.0	28
54	Double Negative Differential Resistance Device Based on Hafnium Disulfide/Pentacene Hybrid Structure. Advanced Science, 2020, 7, 2000991.	11.2	27

#	Article	IF	CITATIONS
55	M-DNA/Transition Metal Dichalcogenide Hybrid Structure-based Bio-FET sensor with Ultra-high Sensitivity. Scientific Reports, 2016, 6, 35733.	3.3	26
56	Effect of large work function modulation of MoS <sub>2</sub> by controllable chlorine doping using a remote plasma. Journal of Materials Chemistry C, 2020, 8, 1846-1851.	5.5	26
57	Poly-4-vinylphenol (PVP) and Poly(melamine- <i>co</i> -formaldehyde) (PMF)-Based Atomic Switching Device and Its Application to Logic Gate Circuits with Low Operating Voltage. ACS Applied Materials & Interfaces, 2017, 9, 27073-27082.	8.0	25
58	Surface Passivation of Germanium Using SF <sub>6</sub> Plasma to Reduce Source/Drain Contact Resistance in Germanium n-FET. IEEE Electron Device Letters, 2015, 36, 745-747.	3.9	23
59	Size-tunable synthesis of monolayer MoS <sub>2</sub> nanoparticles and their applications in non-volatile memory devices. Nanoscale, 2016, 8, 16995-17003.	5.6	23
60	Multifunctional Homogeneous Lateral Black Phosphorus Junction Devices. Chemistry of Materials, 2017, 29, 3143-3151.	6.7	23
61	Analytical Study of Interfacial Layer Doping Effect on Contact Resistivity in Metal-Interfacial Layer-Ge Structure. IEEE Electron Device Letters, 2014, 35, 705-707.	3.9	22
62	Harnessing Recombinant DnaJ Protein as Reversible Metal Chelator for a High-Performance Resistive Switching Device. Chemistry of Materials, 2018, 30, 781-788.	6.7	22
63	High-Efficiency WSe <sub>2</sub> Photovoltaic Devices with Electron-Selective Contacts. ACS Nano, 2022, 16, 8827-8836.	14.6	22
64	Poly-4-vinylphenol and poly(melamine-co-formaldehyde)-based graphene passivation method for flexible, wearable and transparent electronics. Nanoscale, 2014, 6, 3830.	5.6	21
65	Polarity control in a single transition metal dichalcogenide (TMD) transistor for homogeneous complementary logic circuits. Nanoscale, 2019, 11, 12871-12877.	5.6	21
66	Rhenium diselenide (ReSe2) infrared photodetector enhanced by (3-aminopropyl)trimethoxysilane (APTMS) treatment. Organic Electronics, 2018, 53, 14-19.	2.6	20
67	The Efficacy of Metal-Interfacial Layer-Semiconductor Source/Drain Structure on Sub-10-nm n-Type Ge FinFET Performances. IEEE Electron Device Letters, 2014, 35, 1185-1187.	3.9	19
68	Reduction of Threshold Voltage Hysteresis of MoS <sub>2</sub> Transistors with 3-Aminopropyltriethoxysilane Passivation and Its Application for Improved Synaptic Behavior. ACS Applied Materials & Interfaces, 2019, 11, 20949-20955.	8.0	19
69	Twoâ€Ðimensional MXene Synapse for Brainâ€Inspired Neuromorphic Computing. Small, 2021, 17, e2102595.	10.0	19
70	Selective-Area High-Quality Germanium Growth for Monolithic Integrated Optoelectronics. IEEE Electron Device Letters, 2012, 33, 579-581.	3.9	18
71	Controlling Grain Size and Continuous Layer Growth in Two-Dimensional MoS <sub>2</sub> Films for Nanoelectronic Device Application. IEEE Nanotechnology Magazine, 2015, 14, 238-242.	2.0	18
72	Controllable potential barrier for multiple negative-differential-transconductance and its application to multi-valued logic computing. Npj 2D Materials and Applications, 2021, 5, .	7.9	17

#	Article	IF	CITATIONS
73	Photoelectroactive artificial synapse and its application to biosignal pattern recognition. Npj 2D Materials and Applications, 2021, 5, .	7.9	17
74	Asymmetric carrier transport in flexible interface-type memristor enables artificial synapses with sub-femtojoule energy consumption. Nanoscale Horizons, 2021, 6, 987-997.	8.0	16
75	Optimization of graphene-MoS2 barristor by 3-aminopropyltriethoxysilane (APTES). Organic Electronics, 2016, 33, 172-177.	2.6	15
76	Wide-Range Controllable Doping of Tungsten Diselenide (WSe <sub>2</sub> ) based on Hydrochloric Acid Treatment. Journal of Physical Chemistry C, 2017, 121, 14367-14372.	3.1	15
77	Highly Stable Artificial Synapse Consisting of Low-Surface Defect van der Waals and Self-Assembled Materials. ACS Applied Materials & Interfaces, 2020, 12, 38299-38305.	8.0	14
78	Rational Band Engineering of an Organic Double Heterojunction for Artificial Synaptic Devices with Enhanced State Retention and Linear Update of Synaptic Weight. ACS Applied Materials & Interfaces, 2020, 12, 10737-10745.	8.0	14
79	Electrolyteâ€Gated Vertical Synapse Array based on Van Der Waals Heterostructure for Parallel Computing. Advanced Science, 2022, 9, e2103808.	11.2	14
80	Efficient Threshold Voltage Adjustment Technique by Dielectric Capping Effect on MoS <sub>2</sub> Field-Effect Transistor. IEEE Electron Device Letters, 2017, 38, 1172-1175.	3.9	13
81	Versatile Doping Control of Black Phosphorus and Functional Junction Structures. Journal of Physical Chemistry C, 2019, 123, 10682-10688.	3.1	13
82	Fermi-Level Unpinning Using a Ge-Passivated Metal–Interlayer–Semiconductor Structure for Non-Alloyed Ohmic Contact of High-Electron-Mobility Transistors. IEEE Electron Device Letters, 2015, 36, 884-886.	3.9	12
83	Effect of Hydrogen Annealing on Contact Resistance Reduction of Metal–Interlayer–n-Germanium Source/Drain Structure. IEEE Electron Device Letters, 2016, , 1-1.	3.9	11
84	Non-Alloyed Ohmic Contacts on GaAs Using Metal-Interlayer-Semiconductor Structure With SF <sub>6</sub> Plasma Treatment. IEEE Electron Device Letters, 2016, 37, 373-376.	3.9	11
85	Curing temperature- and concentration-dependent dielectric properties of cross-linked poly-4-vinylphenol (PVP). Current Applied Physics, 2013, 13, 1554-1557.	2.4	10
86	Layer-controlled thinning of black phosphorus by an Ar ion beam. Journal of Materials Chemistry C, 2017, 5, 10888-10893.	5.5	9
87	Mixedâ€Dimensional Formamidinium Bismuth Iodides Featuring Inâ€Situ Formed Typeâ€I Band Structure for Convolution Neural Networks. Advanced Science, 2022, 9, e2200168.	11.2	8
88	Effects of Thermal Annealing on In Situ Phosphorus-Doped Germanium \$hbox{n}^{+}/hbox{p}\$ Junction. IEEE Electron Device Letters, 2013, 34, 15-17.	3.9	7
89	Electrical effect of titanium diffusion on amorphous indium gallium zinc oxide. Applied Physics Letters, 2012, 101, .	3.3	6
90	Thin-Film Transistors: High-Performance 2D Rhenium Disulfide (ReS2) Transistors and Photodetectors by Oxygen Plasma Treatment (Adv. Mater. 32/2016). Advanced Materials, 2016, 28, 6984-6984.	21.0	6

#	Article	IF	CITATIONS
91	Temperature-Dependent Electrical Characterization of Amorphous Indium Zinc Oxide Thin-Film Transistors. IEEE Transactions on Electron Devices, 2017, 64, 3183-3188.	3.0	6
92	Reduced graphene oxide produced by rapid-heating reduction and its use in carbon-based field-effect transistors. Journal of Applied Physics, 2012, 112, 033701.	2.5	5
93	Hydrazine-Based Fermi-Level Depinning Process on Metal/Germanium Schottky Junction. IEEE Electron Device Letters, 2013, 34, 599-601.	3.9	5
94	Impact of structural defect density on gettering of transition metal impurities during phosphorus emitter diffusion in multi-crystalline silicon solar cell processing. Electronic Materials Letters, 2015, 11, 658-663.	2.2	5
95	Contact Resistance Reduction Using Dielectric Materials of Nanoscale Thickness on Silicon for Monolithic 3D Integration. Journal of Nanoscience and Nanotechnology, 2016, 16, 12764-12767.	0.9	5
96	Theoretical and Experimental Investigation of Graphene/High-k/p-Si Junctions. IEEE Electron Device Letters, 2016, 37, 4-7.	3.9	5
97	Effects of point defect healing on phosphorus implanted germanium n+/p junction and its thermal stability. Journal of Applied Physics, 2013, 114, .	2.5	4
98	The influence of hydrogenation on the electrical properties of impurity-contaminated silicon grain boundaries. Electronic Materials Letters, 2015, 11, 993-997.	2.2	4
99	Sub 200 °C fluxless indium-tin (In-Sn) eutectic bonding for monolithic 3D-IC. Journal of the Korean Physical Society, 2014, 65, 960-963.	0.7	3
100	The Effect of Post-Fabrication Annealing on an Amorphous IGZO Visible-Light Photodetector. Journal of Nanoscience and Nanotechnology, 2016, 16, 11745-11749.	0.9	3
101	An Optogeneticsâ€Inspired Flexible van der Waals Optoelectronic Synapse and its Application to a Convolutional Neural Network (Adv. Mater. 40/2021). Advanced Materials, 2021, 33, 2170316.	21.0	3
102	Characteristics of Ultrashallow Hetero Indium–Gallium–Zinc–Oxide/Germanium Junction. IEEE Electron Device Letters, 2012, 33, 1363-1365.	3.9	2
103	Negative effect of Au nanoparticles on an IGZO TFT-based nonvolatile memory device. Journal of the Korean Physical Society, 2014, 64, 337-340.	0.7	2
104	Graphene: Extremely Low Contact Resistance on Graphene through nâ€īype Doping and Edge Contact Design (Adv. Mater. 5/2016). Advanced Materials, 2016, 28, 975-975.	21.0	2
105	Photodetectors: Highâ€Performance Transition Metal Dichalcogenide Photodetectors Enhanced by Selfâ€Assembled Monolayer Doping (Adv. Funct. Mater. 27/2015). Advanced Functional Materials, 2015, 25, 4368-4368.	14.9	1
106	Photodetectors: Broad Detection Range Rhenium Diselenide Photodetector Enhanced by (3-Aminopropyl)Triethoxysilane and Triphenylphosphine Treatment (Adv. Mater. 31/2016). Advanced Materials, 2016, 28, 6518-6518.	21.0	1
107	Impact of Metal Nitrides on Contact Resistivity of Metal-Interlayer-Semiconductor Source/Drain in Sub-14 nm n-Type Si FinFET. Journal of Nanoscience and Nanotechnology, 2017, 17, 3084-3088.	0.9	1
108	Characterization of Geometric Leakage Current of \$ hbox{GeO}_{2}\$ Isolation and Effect of Forming Gas Annealing in Germanium p-n Junctions. IEEE Electron Device Letters, 2012, 33, 1520-1522.	3.9	0

#	Article	IF	CITATIONS
109	Dopant profile model in a shallow germanium n+/p junction. Journal of the Korean Physical Society, 2013, 63, 1855-1858.	0.7	0
110	Experimental and Theoretical Analysis of Cu Diffusion in Cu-Induced Germanium Crystallization. Journal of Nanoscience and Nanotechnology, 2016, 16, 12900-12903.	0.9	0
111	Characteristics of Nano-Laminated Al-Doped ZnO (AZO) Multilayers. Journal of Nanoscience and Nanotechnology, 2016, 16, 11715-11721.	0.9	0
112	Residue-Free Silver Nano Patterns Fabricated by Reverse Direct Imprinting. Journal of Nanoscience and Nanotechnology, 2016, 16, 12983-12987.	0.9	0
113	The Effects of a Thermal Recovery Process in In-Ga-Zn-O (IGZO) Thin Films Transistor. Journal of Nanoscience and Nanotechnology, 2016, 16, 11509-11512.	0.9	0
114	Spatial Control of Photoacid Diffusion in Chemically Amplified Resist (CAR) via External Electric Field. Journal of Nanoscience and Nanotechnology, 2018, 18, 6001-6004.	0.9	0
115	Effects of Cu Ion Doping in HfO2-Based Atomic Switching Devices. Journal of Nanoscience and Nanotechnology, 2017, 17, 7297-7300.	0.9	0
116	Strained Polycrystalline Germanium by Metal-Induced Layer Exchange Crystallization. Journal of Nanoscience and Nanotechnology, 2017, 17, 7628-7631.	0.9	0